Cell Reports

Report

PRDX1 Counteracts Catastrophic Telomeric Cleavage Events That Are Triggered by DNA Repair Activities Post Oxidative Damage

Graphical Abstract

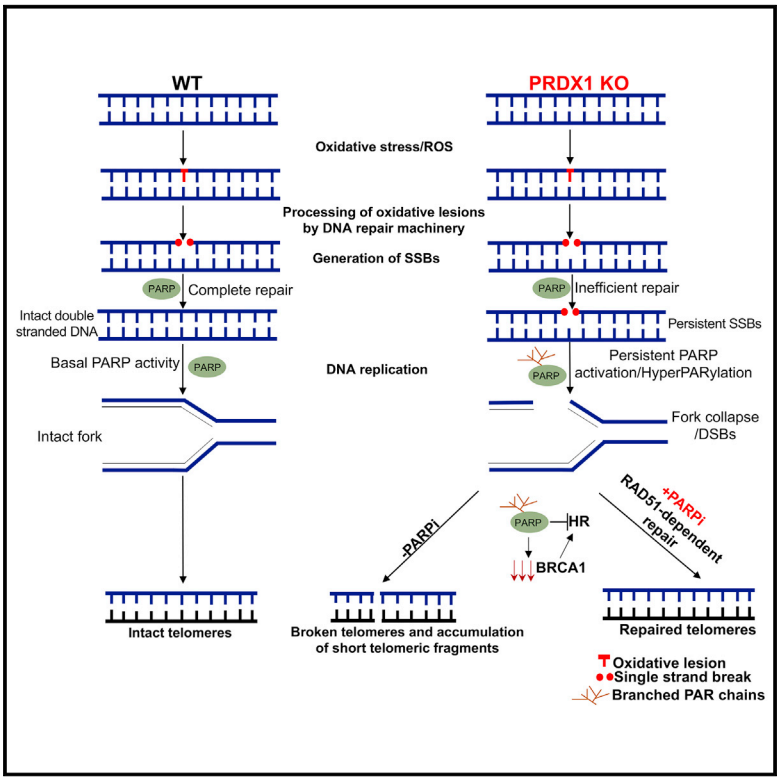

Highlights

- PRDX1 suppresses oxidative stress-induced single-strand breaks (SSBs) at telomeres
- *PRDX1*-KO cells accumulate telomeric SSBs after oxidative damage by DNA processing
- Persistent SSBs are converted into DSBs in a replication-dependent manner
- PARP inhibition promotes RAD51-dependent repair of damaged telomeres

Authors

Wareed Ahmed, Joachim Lingner

Correspondence

wareed.ahmed@ki.se (W.A.),
joachim.lingner@epfl.ch (J.L.)

In Brief

Ahmed and Lingner demonstrate that oxidative stress in cancer cells lacking the antioxidant enzyme PRDX1 leads to incomplete PARP1-dependent DNA repair, resulting in catastrophic telomere loss events upon DNA replication. Drug-mediated PARP1-inhibition counteracts telomere loss, favoring telomere repair by RAD51-dependent homologous recombination.

Ahmed & Lingner, 2020, Cell Reports *33*, 108347
November 3, 2020
https://doi.org/10.1016/j.celrep.2020.108347

CellPress

Cell Reports

CellPress
OPEN ACCESS

Report

PRDX1 Counteracts Catastrophic Telomeric Cleavage Events That Are Triggered by DNA Repair Activities Post Oxidative Damage

Wareed Ahmed[1,2,*] and Joachim Lingner[1,3,*]

[1]Swiss Institute for Experimental Cancer Research (ISREC), School of Life Sciences, Ecole Polytechnique Fédérale de Lausanne (EPFL), 1015 Lausanne, Switzerland

[2]Present address: Department of Medical Biochemistry and Biophysics, Karolinska Institutet, SciLifeLab, 17165 Stockholm, Sweden

[3]Lead Contact

*Correspondence: wareed.ahmed@ki.se (W.A.), joachim.lingner@epfl.ch (J.L.)

https://doi.org/10.1016/j.celrep.2020.108347

SUMMARY

Telomeres are prone to damage inflicted by reactive oxygen species (ROS). Oxidized telomeric DNA and nucleotide substrates inhibit telomerase, causing telomere shortening. In addition, ROS can induce telomeric single-strand DNA breaks (SSBs). The peroxiredoxin-PRDX1 is enriched in telomeric chromatin and this counteracts ROS-induced telomere damage. Here, we identify DNA processing after oxidative stress as a main source of telomeric DNA cleavage events in the absence of PRDX1. In PRDX1-depleted cells, poly(-ADP-ribose) polymerase (PARP)-dependent telomeric repair is often incomplete, giving persistent SSBs that are converted into telomeric double-strand breaks during replication, leading to rapid telomere shortening. Interestingly, PARP1 inhibition dampens telomere shortening, triggering stabilization of the homologous recombination (HR) factor BRCA1 and RAD51-mediated repair of telomeres. Overall, our results reveal that, in the absence PRDX1, incomplete PARP1-dependent DNA repair and competition between PARP1 and HR cause ROS-induced telomeric catastrophe.

INTRODUCTION

Oxidative stress mediated by reactive oxygen species (ROS) has an important role in tumorigenesis and cancer progression (Sotgia et al., 2011). A wide range of chemicals, UV light, and ionizing radiation generates ROS. In addition to external sources, ROS is induced endogenously mostly during oxygen-consuming metabolic reactions in mitochondria; during oxidative phosphorylation, electrons can leak, causing partial oxygen reduction into superoxide radicals (O_2-·). Superoxide radicals are converted into H_2O_2, which, in turn, can decay into hydroxyl radicals. Excessive ROS production damages cellular components, including proteins, DNA, and lipids. Notably, several anti-cancer therapies act by generating ROS, and upregulation of ROS scavenging anti-oxidant proteins can reduce the therapeutic response (Yang et al., 2018).

ROS have the potential to oxidize free nucleotides and DNA bases. In addition, ROS can lead to single-strand breaks (SSBs) in the DNA backbone. These may be generated either by ROS directly or indirectly by the processing of oxidized nucleobases by DNA repair proteins (Caldecott, 2008). Processing of SSBs involves repair proteins, which are orchestrated at the site of DNA damage by the poly(ADP)-ribose polymerases PARP1 and PARP2. PARP1 acts as a sensor of DNA breaks and rapidly associates with sites of damage, where it adds poly (ADP)-ribose moieties from donor NAD^+ molecules on itself and other target proteins (Satoh and Lindhal, 1992; Eustermann et al., 2015). One of the targets of PARP1 is XRCC1, which acts as a scaffold for SSB repair proteins, including ligase 3, polymerase β, and polynucleotide kinase 3′ phosphatase (PNKP) (El-Khamisy et al., 2003). Depletion of PARP1 or inhibition of PARylation strongly delays SSB repair (Fisher et al., 2007). Failure to repair SSBs because of defects in the repair system or excessive damage load overwhelming the repair capacity in proliferating cells causes blockage or collapse of replication forks leading to the generation of potentially lethal double-strand breaks (DSBs) (Kuzminov, 2001). DSBs are repaired either by error-prone non-homologous end joining (NHEJ) or the high-fidelity template-dependent homologous recombination (HR) repair pathway. The choice between repair pathways is governed by cell cycle stages and chromatin features (Ceccaldi et al., 2016). Repair of DSBs by HR involves many proteins, including BRCA1, which facilitates processing of DSBs and which, in collaboration with BRCA2, mediates the loading of the HR recombinase RAD51 onto DNA. The SSB and HR repair pathways both cooperate to maintain genome stability. Hence, the induction of persistent SSBs by inhibition of PARP1 in HR-defective cells leads to genomic catastrophe and cell death (Farmer et al., 2005; Bryant et al., 2005). This feature is referred to as synthetic lethality and is exploited in the clinic using PARP inhibitor (PARPi)-based treatment of BRCA-negative ovarian cancers (Lord and Ashworth, 2017). Notably, in addition to its roles in SSB repair, PARP1 also contributes to DNA damage signaling

and repair of DSBs, but that function is not well understood (Ray Chaudhuri and Nussenzweig, 2017).

The cellular armory of anti-oxidant enzymes includes catalase, glutathione peroxidases, and peroxiredoxins (PRDXs) (Perkins et al., 2015). They reduce ROS levels and consequently suppress the accumulation of oxidative lesions, thereby preventing genomic instability. Upregulation of anti-oxidant proteins in cancer cells confers resistance to chemo- and radio-therapy (Kim et al., 2008; Diehn et al., 2009). PRDXs exhibit peroxidase activity and regulate the intracellular levels of hydroxyl radicals by reducing H_2O_2 into water. In addition to performing an oxidant-detoxification function, PRDXs are implicated in stabilizing target proteins during exposures to high levels of oxidants as well as in transduction of redox signals to downstream target proteins (redox switch activity) (Perkins et al., 2015; Neumann et al., 2009). High expression of PRDXs is associated with resistance to radio- and chemotherapy, which may be an attribute of its ROS scavenging ability (Chung et al., 2001; Noh et al., 2001; Park et al., 2006). In *prdx1* knockout (KO) mice, increased incidence of tumor formation, reduced lifespan, enhanced susceptibility to oxidative DNA damage, and increased likelihood of loss of heterozygosity support an association of PRDX1 with genomic stability (Neumann et al., 2003).

Telomeres are nucleoprotein complexes that act as protective caps at chromosomes ends shielding them from degradation, DNA recombination, DNA end joining, and the DNA damage response (DDR). Human telomeres are composed of 5–15-kb-long 5′-TTAGGG-3′/5′-CCCTAA-3′ repeats terminating in 50–200-nt-long G-rich 3′ single-stranded overhangs. Telomeres are associated with the six-subunit-containing shelterin complex, which represses DDR signaling at telomeres and prevents illegitimate repair (de Lange, 2009; Lazzerini-Denchi and Sfeir, 2016). The sequence and structure of telomeres make them susceptible to ROS-mediated cleavage and base oxidation (reviewed by Ahmed and Lingner [2018a] and von Zglinicki [2002]). *In vitro* studies have shown that ROS preferentially cleaves oligonucleotides containing telomeric sequences (Oikawa and Kawanishi 1999). Oxidative lesions in the single-stranded regions of telomeres are considered irreparable because the base excision repair (BER) system requires a complementary template DNA to replace modified bases. Moreover, the above problems are further compounded by the repression of DDR and repair at telomeres, allowing some damage to remain undetected, causing their persistence (Coluzzi et al., 2014). Therefore, maintaining the stability of oxidative-damage-sensitive telomeres may demand robust anti-oxidant defense systems, which upfront prevent the formation of oxidative lesions.

The consequences of persistent oxidative lesions on telomere integrity are not well understood. In our earlier studies, we identified the association of PRDX1 with telomeric chromatin during S and G2 phases of the cell cycle (Aeby et al., 2016). We also showed that PRDX1, in collaboration with the deoxyribonucleotide triphosphohydrolase (dNTPase) MTH1, suppresses the accumulation of 8-oxo-2′-deoxyguanosine (8-oxo-dG) into nuclear DNA (Ahmed and Lingner, 2018b). Importantly, it has been shown that 8-oxo-2′-deoxyguanosine triphosphate (8-oxo-dGTP), when added by telomerase, acts as a chain terminator, whereas 8-oxo-dG, when present within a DNA substrate, may either inhibit or stimulate telomerase activity in *vitro*, depending upon its location in the telomeric DNA sequence (Fouquerel et al., 2016; Aeby et al., 2016). Therefore, PRDX1 and MTH1 are critical for telomere length maintenance in live cells (Ahmed and Lingner, 2018b).

Here, we characterize mechanisms that lead, upon oxidative stress, to SSBs and DSBs at telomeres in *PRDX1* KO cells. We find that SSBs are generated after oxidative stress because of DNA processing. SSBs are only partially repaired, in a PARP-dependent manner, and converted into DSBs, upon replication, leading to frequent telomere truncations. Surprisingly, DSB repair by RAD51-dependent HR becomes more effective upon inhibition of PARylation. In PRDX1-deficient cells, ROS leads to BRCA1 destabilization in a PARP1-dependent manner. Thus, massive telomere damage in the absence of PRDX1 leads to incomplete DNA repair and competition among DNA-repair pathways, which cause massive telomere instability.

RESULTS

ROS Induces Telomeric SSBs after Oxidative Stress, Which Persist in PRDX1-Depleted Cells

In our earlier study, we observed with oxidative stress the formation of telomeric SSBs in HT1080 fibrosarcoma and HCT116 colon cancer cells in which the *PRDX1* gene had been knocked out (Aeby et al., 2016). To understand the underlying mechanisms, we treated HCT116 wild-type (WT) and *PRDX1* KO cells with the drug menadione, which perturbs mitochondrial function and triggers ROS generation (Gerasimenko et al., 2002; Loor et al., 2010). After drug treatment for 30 min, cells were allowed to recover in fresh medium for 3 h (scheme of assay in Figure S1A). Genomic DNA was isolated and digested with restriction enzymes, and the integrity of telomeric DNA was analyzed by southern hybridization on native gels to monitor DSBs as well as on alkaline denaturing gel to detect SSBs. The analysis of telomeric DNA on native gels in WT and *PRDX1* KO cells did not show telomere DSBs (Figures S1B and S1C). However, the analysis of the same samples on alkaline-denaturing gels revealed, in two different *PRDX1* KO clones with different telomere lengths, the presence of SSBs, which increased further during the recovery period (Figures S1D and S1E). We reasoned that the progressive increase in SSBs in *PRDX1* KO cells might have been the consequence of irreversible damage of mitochondria by menadione leading to continuous release of ROS, inflicting continuous damage during the recovery. To test this possibility, we added the well-established anti-oxidant N-acetyl-cysteine (NAC), which scavenges ROS (Dekhuijzen, 2004), to the recovery medium. Addition of NAC before menadione treatment suppressed the telomeric damage (Figures S1F, S1G, lanes 4 and 9, and S1H), validating that the ROS-mediated damage upon menadione treatment was efficiently repressed with NAC. In WT cells, NAC addition after the treatment allowed efficient repair of SSBs during the 3 h recovery period. However, in *PRDX1* KO cells, NAC addition during the recovery period did not facilitate repair. Instead, SSBs persisted, indicating a failure in SSB repair (Figures 1A and 1B).

To corroborate these results, we repeated the experiments treating cells with the oxidant H_2O_2. Analysis of telomeric DNA isolated from H_2O_2-treated cells at different time intervals

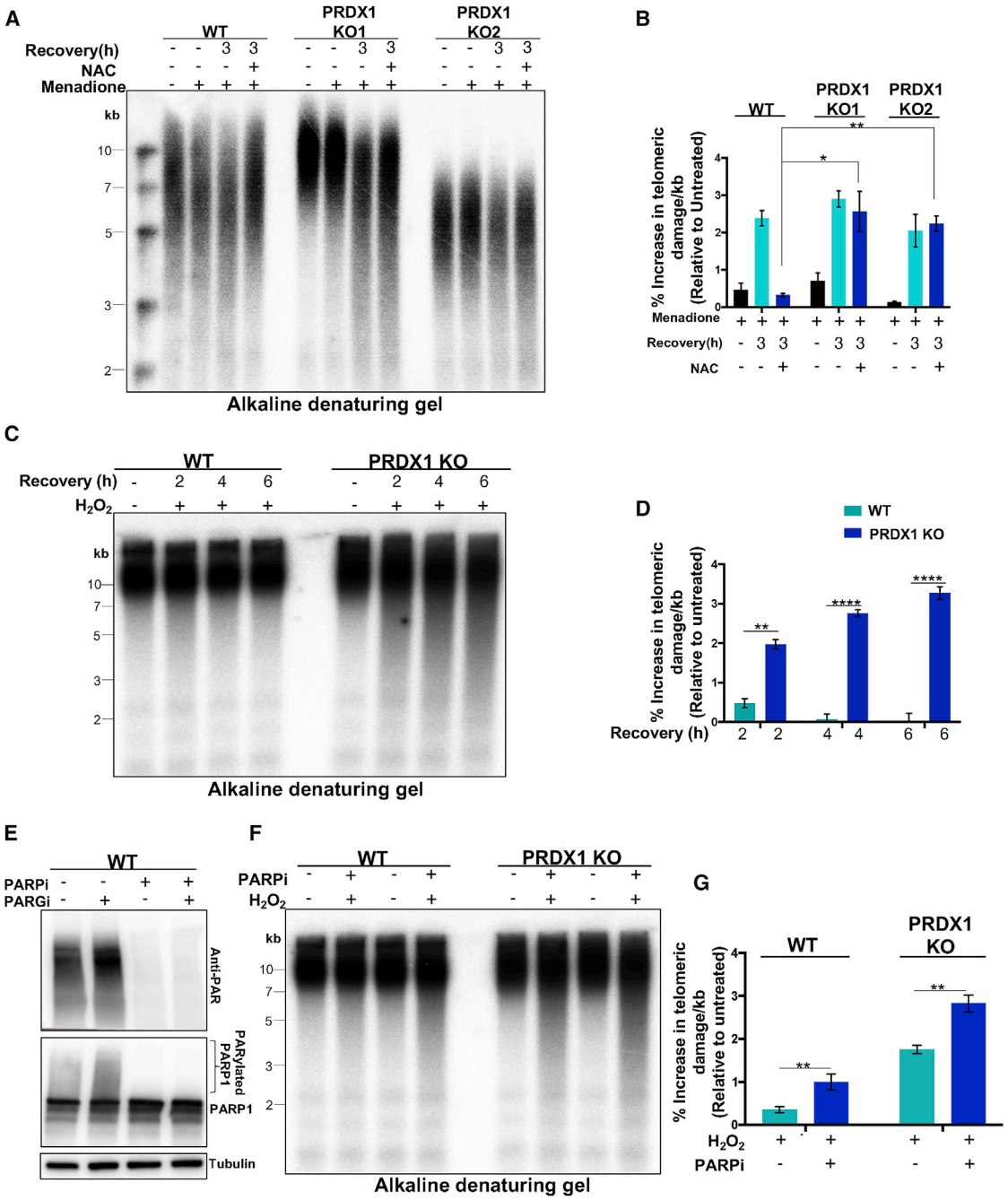

Figure 1. Oxidative Stress Triggers Persistent Single-Strand Breaks (SSBs) at Telomeres in *PRDX1* KO Cells

(A) Analysis of ROS-induced SSBs at telomeres on alkaline-denaturing gel. HCT116 cells were treated with menadione for 30 min and were recovered in complete DMEM with or without the anti-oxidant N-acetyl cysteine (NAC). Telomeric DNA fragments were detected with a telomere-specific probe.

(B) Quantification of telomeric damage from (A). SDs were obtained from two independent experiments. *$p < 0.05$, **$p < 0.01$; unpaired two-tailed Student's t test.

(C) Alkaline gel analysis of H_2O_2-induced SSBs at telomeres at different time intervals as indicated in the figure. HCT116 cells treated with 1 mM H_2O_2 for 30 min, followed by recovery in complete DMEM supplemented with NAC.

(D) Quantification of telomeric damage from (C). SDs were obtained from three independent experiments. **$p < 0.01$, ****$p < 0.0001$; unpaired two-tailed Student's t test.

(E) Immunoblot analysis of total PARylation and specific PARylation of PARP1 using anti-PAR and anti-PARP1 antibodies, respectively. PARP inhibitor talazoparib (1 μM), and PARG inhibitor ADP-HPD (1 μM), were used to inhibit PARylation and degradation of existing PARylation, respectively. Tubulin was used as a loading control.

(F) Analysis of telomeric SSBs on alkaline-denaturing gel. HCT116 cells treated with 1 mM H_2O_2 for 30 min. After the treatment, cells were recovered for 2 h in NAC containing DMEM with DMSO or 1 μM PARP inhibitor Talazoparib.

(G) Quantification of telomeric damage from (C). SDs were obtained from three independent experiments. **$p < 0.01$; unpaired two-tailed Student's t test.

confirmed that SSBs accumulated during the recovery period in *PRDX1* KO cells, whereas in WT cells, the damage was repaired efficiently (Figures 1C, 1D, and S2A). In addition, we observed accumulation of SSBs in HeLa cells in which PRDX1 was depleted by short hairpin RNA (shRNA), indicating that the effect was not cell line specific (Figure S2B). Importantly, the depletion of the oxidative lesion processing DNA glycosylase OGG1 led to a significant reduction in SSB generation during the recovery period, whereas progressive increases in SSBs were observed in OGG1-proficient *PRDX1* KO cells treated with H_2O_2 (Figures S2C–S2E). Overall, the accumulation of SSBs in *PRDX1* KO cells after oxidative stress indicated that SSBs are generated by DNA processing involving OGG1.

PARP Activity Promotes SSBs Repair at Telomeres

PARP1 and PARP2 act as sensors of DNA breaks, and upon encountering SSBs, they promote PARylation-dependent recruitment of downstream repair proteins (Hanzlikova et al., 2017). To assess the role of PARP on the repair of oxidative-stress-induced SSBs at telomeres, we treated cells with the PARP inhibitor (PARPi) Talazoparib. Western blot analysis revealed that, at 1 μM, Talazoparib abolished the PARylation of cellular proteins as well as PARylation of PARP1 (Figure 1E). The cells were treated with H_2O_2, and PARPi was added to the recovery medium. After 2 h of recovery, telomeric DNA was fractionated on alkaline denaturing gels and hybridized with a telomeric probe to detect telomeric SSBs. Presence of PARPi during the recovery period increased the levels of H_2O_2-induced telomeric SSBs in both WT and *PRDX1* KO cells, and as seen before, the levels of SSBs were higher in *PRDX1* KO cells (Figures 1F and 1G). To further evaluate the effect of PARP trapping by PARP inhibitors on the repair of SSBs, we treated cells with veliparib, olaparib, and talazoparib, which possess variable PARP-trapping activities. Interestingly, the accumulation of SSBs was the highest with talazoparib and the lowest with veliparib, correlating with the PARP-trapping ability of PARP inhibitors (Figures S2F and 2G). These results indicate that PARP trapping on damaged DNA interferes with SSB repair at telomeres.

Oxidative-Stress-Induced, Persistent SSBs Give Rise to Short Telomeric Fragments in a Replication-Dependent Manner in *PRDX1* KO Cells

Inefficient repair of SSBs is expected to have deleterious consequences in proliferating cells because SSBs become converted into DSBs during DNA replication (Figure 2A). To assess the consequences of SSB accumulation in *PRDX1* KO cells on telomere maintenance, we treated cells with H_2O_2 and allowed them to recover in fresh medium for 20 h before analyzing telomeric DNA on native gels (Figure 2B). Terminal restriction fragment (TRF) length analysis showed the appearance of short telomeric DNA fragments in H_2O_2-treated *PRDX1* KO cells, whereas damage was barely detectable in WT cells (Figures 2D and 2E). Further, the analysis of undigested genomic DNA and the comparison to total genome or Alu-repeat DNA suggested that damage occurred preferentially at telomeres and that the short telomeric fragments were extrachromosomal (Figure S3A). To understand the origin of the short telomeric fragments, we treated cells with thymidine, which is an inhibitor of DNA synthesis as it leads to depletion of deoxycytidine triphosphate (dCTP) (an effect known as thymidine block [Bjursell and Reichard, 1973]). Treatment of cells with thymidine inhibited the incorporation of thymidine analog 5-ethynyl-2′-deoxyuridine (EdU) into DNA, suggesting successful imposition of the replication blockade (Figure 2C). At the same time, the appearance of short telomeric fragments was suppressed (Figures 2D and 2E), indicating that telomere truncations were generated during DNA replication upon conversion of SSBs into DSBs. The accumulation of DNA damage at telomeres in *PRDX1* KO cells, which were actively replicating and exposed to H_2O_2, was further confirmed in chromatin immunoprecipitation (ChIP) experiments demonstrating the association of the DNA damage marker γH2AX with telomeric DNA (Figures 2F and 2G).

PARP Inhibition or PARP1 Depletion Suppresses the Generation of ROS-Induced Short Telomeric Fragments

PARP inhibition increased the levels of telomeric SSBs in H_2O_2-treated *PRDX1* KO cells, which provoked us to assess the levels of double-stranded short telomeric fragments upon PARP inhibition or depletion. PARP activity was inhibited with talazoparib, and PARP1 was depleted with small interfering RNA (siRNA) (Figure 3A). PARP1 accounts most PARylation activity in response to DNA damage (Beck et al., 2014). Cells transfected with control siRNA (siGFP) or siPARP1 were treated with H_2O_2 and allowed to recover in fresh medium containing DMSO or PARPi. Telomeric DNA was analyzed after 20 h of recovery (Figure 3B). Unexpectedly, addition of PARP inhibitor or depletion of PARP1 strongly reduced the levels of short telomeric DNA fragments in *PRDX1* KO cells and reduced the presence of γH2AX at telomeres (Figures 3C–3F). Cell cycle analysis did not reveal any notable difference between H_2O_2-treated and H_2O_2+PARPi-treated cells (Figure S3B). Therefore, PARP1 activity appeared to promote, rather than suppress, the generation of telomeric DSBs.

Inhibition of PARP Activity Stimulates RAD51-Dependent Repair at Telomeres

Because PARP inhibition suppressed the accumulation of short double-stranded telomeric DNA fragments in *PRDX1* KO cells, we hypothesized that inhibition of PARP1 may stimulate DSB repair at telomeres. HR repairs DSBs during S and G2 phases, and it rescues collapsed replication forks throughout the genome (Saada et al., 2018; Figure 4A) as well as at telomeres (Doksani and de Lange, 2016; Fouquerel et al., 2019). To test the involvement of the RAD51 recombinase for the repair of oxidative-damage-induced telomeric DSBs in PARPi treated cells, we added a RAD51 inhibitor at a concentration that inhibited the formation of irradiation (IR)-induced RAD51 foci (Figure S4A) to cells that had been treated with H_2O_2 and PARPi. Strikingly, RAD51 inhibition partially reinstated the appearance of short telomeric DNA fragments, suggesting that inhibition of PARP activity triggers RAD51-dependent repair of damaged telomeres (Figures 4B, 4C, and S4B–S4D). Similar to RAD51 inhibition, depletion of RAD51 (Figures S4E–S4G) resulted in reappearance of short telomeric DNA fragments in PARPi- and

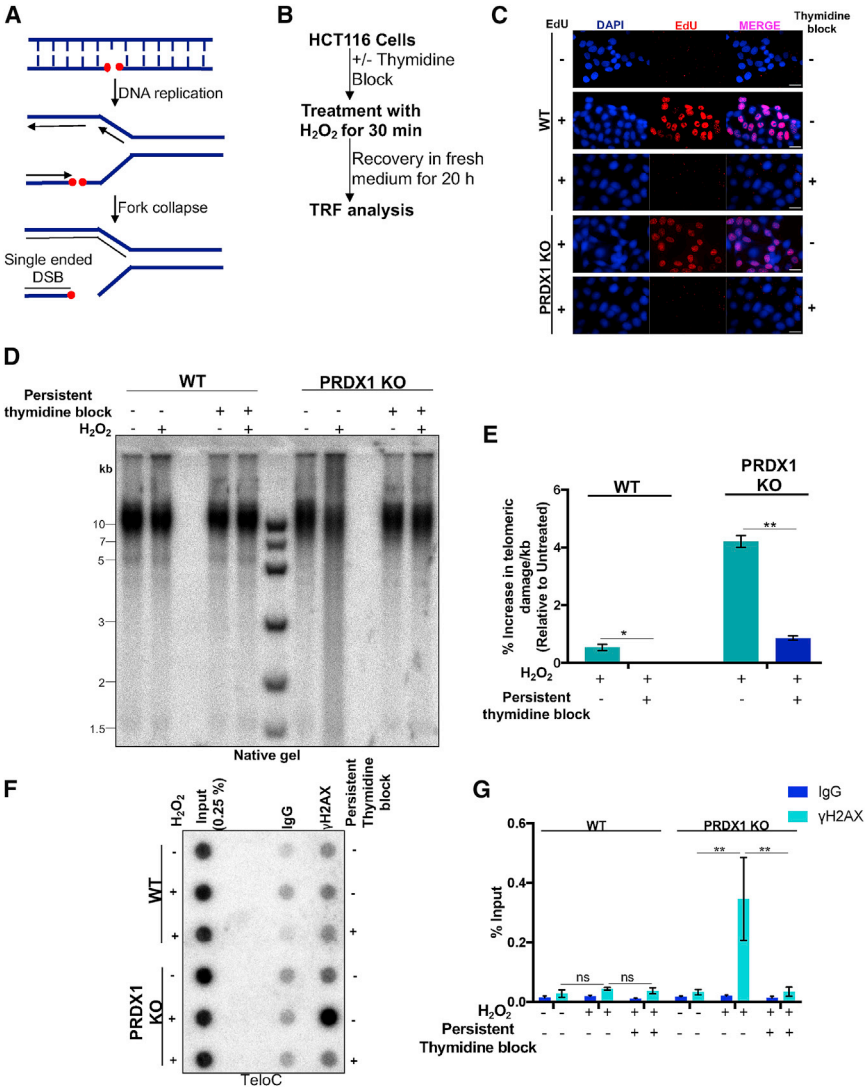

Figure 2. Replication-Dependent Generation of Double-Strand Breaks (DSBs) in *PRDX1* KO Cells upon Oxidative Stress

(A) Schematic representing the replication-dependent conversion of SSBs into DSBs.

(B) Scheme of the assay for analyzing the effect of DNA replication on ROS-induced telomeric DSBs.

(C) Detection of EdU incorporation by fluorescence microscopy to detect thymidine-mediated blocking of DNA replication. Cells treated with or without thymidine were incubated with EdU for 2 h, followed by analysis of its incorporation into DNA. Scale bar, 20 μm.

(D) Monitoring of H_2O_2-induced short telomere fragments on native gel by southern hybridization. Telomeric DNA fragments were visualized with a telomere-specific probe (TeloC).

(E) Quantification of telomeric damage from (D). SDs were obtained from three independent experiments. *p < 0.05, **p < 0.01; unpaired Student's t test.

(F) ChIP analysis of γH2AX at telomeres. The ChIP DNA was spotted on the membrane and probed with a telomere-specific probe (TeloC) to visualize telomeric DNA.

(G) Quantification of (F). SDs were obtained from three independent experiments. ns = p > 0.05, **p < 0.01, **p < 0.01; unpaired Student's t test.

H_2O_2-treated *PRDX1* KO cells. We performed RAD51-ChIP to detect the presence of RAD51 at telomeres. Inhibition of PARP leads to increased association of RAD51 with telomeres of *PRDX1* KO cells that were exposed to oxidative stress (Figures 4D and 4E). Notably, addition of RAD51 inhibitor or depletion of RAD51 in H_2O_2-treated *PRDX1* KO cells did not enhance the levels of telomeric DSBs, indicating that RAD51 repair pathways are defective in *PRDX1* KO cells under oxidative stress (Figures S4B–S4D and S4E–S4G). Together, these results suggest that, in *PRDX1* KO cells, RAD51-dependent DSB repair is repressed at telomeres by PARP.

One of the essential components of HR is BRCA1, which has been shown to be regulated by PARP1 activity during HR repair (Hu et al., 2014). This previous observation provoked us to measure BRCA1 levels in WT and *PRDX1* KO cells upon oxidant treatment. The immunoblot analysis showed that oxidant treatment strongly reduced the levels of BRCA1 in *PRDX1* KO cells compared with WT cells, in which only a slight decrease in BRCA1 levels was observed (Figures 4F and 4G). Importantly, addition of anti-oxidant NAC before H_2O_2 treatment or PARP inhibitor significantly rescued the BRCA1 levels, correlating with the stimulation of HR-dependent repair of telomeres upon PARP inhibition. Inhibition of the proteasome with MG132 did not rescue BRCA1 levels (Figure 4F). Transcript abundance of BRCA1 also remained unaltered in both the WT and *PRDX1* KO cells indicating a post-transcriptional regulatory mechanism by PARP (Figure 4H). Altogether, these results revealed that oxidative stress in *PRDX1* KO cells leads to PARylation-mediated repression of HR, resulting in replication-dependent accumulation of DSBs at telomeres (Figure S5).

DISCUSSION

Telomere maintenance is essential for all proliferating cells for maintaining an intact chromosome structure. Telomeres are considered particularly susceptible to ROS-induced damage (Ahmed and Lingner, 2018a). Recently, we have shown that oxidative stress in cancer cells can lead to telomere shortening by inhibiting the activity of the telomere-length maintenance-enzyme telomerase (Ahmed and Lingner, 2018b). This effect was particularly pronounced upon loss of PRDX1 and MTH1. In addition to inhibiting telomerase activity, oxidative stress also promotes accumulation of SSBs at telomeres, which may contribute to telomere shortening in proliferating cells. Accordingly, addition of anti-oxidants

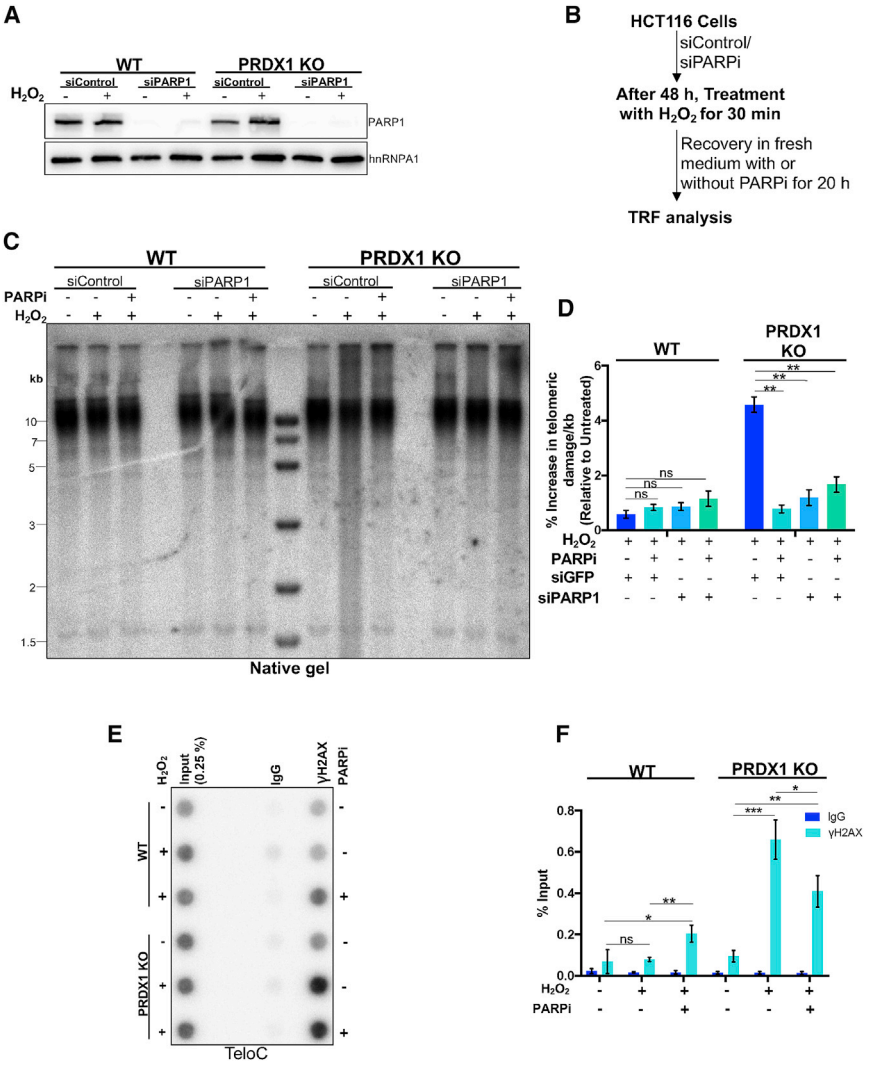

Figure 3. PARP Inhibition or Depletion of PARP1 Suppresses the Accumulation of ROS-Induced Short Telomeric Fragments in *PRDX1* KO Cells

(A) Immunoblot analysis of PARP1 levels in siControl or siPARP1-transfected cells. hnRNAP1 represents the loading control.

(B) Scheme of the assay for analyzing the effect of siPARP1 or PARPi on oxidative-stress-induced telomeric DNA damage.

(C) Detection of telomeric integrity by TRF gel analysis. siControl and siPARP1-transfected cells were treated with H_2O_2 and, after treatment, were recovered for 20 h in anti-oxidant-containing medium in the presence and absence of 1 μM of PARP inhibitor Talazoparib.

(D) Quantification of (C). SDs were obtained from two independent experiments. ns = $p > 0.05$, **$p < 0.01$; unpaired two-tailed Student's t test.

(E) ChIP analysis of the γH2AX accumulation at telomeres. The ChIP DNA was spotted by dot blot, and the membrane was probed with a telomere-specific probe (TeloC) to visualize telomeric DNA.

(F) Quantification of (E). SDs were obtained from three independent experiments. ns = $p > 0.05$, *$p < 0.05$, **$p < 0.01$; unpaired Student's t test.

has been shown to suppress the accumulation of telomeric SSBs and reduce the rate of telomere shortening (von Zglinicki 2002).

In a previous study, we found that PRDX1 associates with telomeric chromatin. In response to oxidative stress PRDX1 binding to telomeres increases and *PRDX1* KO cells exhibit higher levels of SSBs at telomeres, which was attributed to its ROS-scavenging ability (Aeby et al., 2016). Here, we show that ROS-induced SSBs are mostly generated, not by ROS directly, but by DNA processing of presumably oxidized bases during base-excision repair (Figure S5). Furthermore, inhibition of PARP1 delayed the repair of SSBs in WT cells and further enhanced the telomeric SSBs in *PRDX1* KO cells. These observations highlight the importance of PRDX1 in preventing massive telomere damage, which yields persistent SSBs because of incomplete repair (Figure S5). Interestingly, over time, these persistent SSBs give rise to extremely short telomeric fragments upon DNA replication. We find that the accumulation of these short telomeric fragments occurs because of the deficiency of the DSB DNA repair pathway that involves RAD51 and BRCA1.

We observed that DSB repair is inhibited by PARP1, and PARP1 inhibition rescued the oxidative-stress-mediated reduction in BRCA1 levels, promoting RAD51-dependent repair of damaged telomeres.

Previous work demonstrated that DSBs within telomeric repeats are repaired by both HR and PARP1-dependent alt-NHEJ (Doksani and de Lange, 2016). Therefore, alt-NHEJ and HR compete for the same damaged DNA substrates, and upon inhibition of PARP1, the HR pathway is favored, which is seen here to occur by the stimulation of RAD51-dependent repair upon inhibition of PARP. Several publications provided evidence that PARP can interfere with HR. Inhibition of PARP1 activity or PARP1 depletion results in a hyper-recombinogenic phenotype, coinciding with increased levels of sister chromatid exchange and a higher number of RAD51 foci (Schultz et al., 2003). In addition, PARP1 antagonizes DNA resection at sites of DSBs, which precedes loading of RAD51 and invasion into the repair template. PARP1 loss led to reduced recruitment of the resection inhibitors KU, 53BP1, and RIF1, promoting hyper-resection and HR (Caron et al., 2019). Another mechanism proposed to describe PARP1-dependent repression of HR involves BRCA1. PARylated BRCA1 is recognized by receptor-associated protein 80 (RAP80), which stabilizes the BRCA1-RAP80 complex and limits HR. Loss of BRCA1 PARylation elevated recombination, suggesting that PARP1 negatively regulates HR (Hu et al., 2014).

Treatment of *PRDX1* KO cells with oxidant resulted in reduced BRCA1 levels, which could be rescued upon inhibition of PARP1,

CellPress
OPEN ACCESS

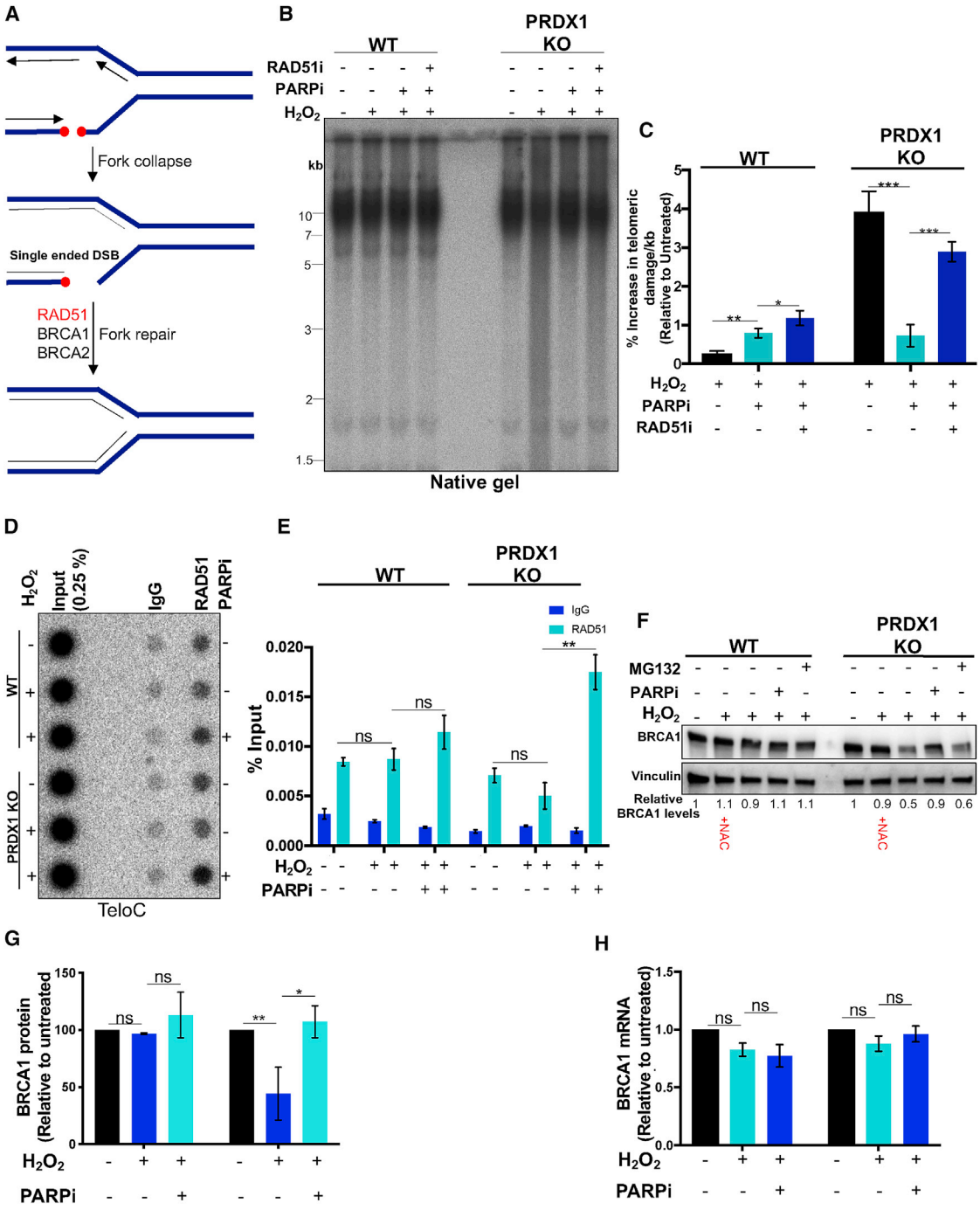

Figure 4. Inhibition of PARP Stimulates RAD51-Dependent Repair and Rescues BRCA1 Levels

(A) Schematic representation of the repair of a collapsed replication fork by homologous recombination.

(B) Detection of telomeric DNA integrity by TRF analysis.

(C) Quantification of telomeric damage from (B). SDs were obtained from three independent experiments. *$p < 0.05$, **$p < 0.01$, ***$p < 0.001$; unpaired Student's t test.

(D) ChIP analysis of RAD51 at telomeres. The ChIP DNA was spotted on a membrane probed with a telomere-specific probe (TeloC) to visualize telomeric DNA.

(E) Quantification of (D). SDs were obtained from two independent experiments. ns = $p > 0.05$,**$p < 0.01$; unpaired Student's t test.

(F) Immunoblot analysis of BRCA1 levels 6 h after H_2O_2 treatment. Vinculin was used as a loading control. +NAC lanes represent the samples from cells that were incubated with anti-oxidant NAC before the exposure to H_2O_2. Proteasomal inhibitor MG132 (20 μM) was added 6 h before H_2O_2 treatment and maintained in the recovery medium.

(G) Quantification of BRCA1 protein levels. SDs were obtained from three independent experiments. ns = $p > 0.05$, *$p < 0.05$, **$p < 0.01$; unpaired Student's t test.

(H) Measurement of BRCA1 mRNA by quantitative real-time RT-PCR. SDs were obtained from three independent experiments. ns = $p > 0.05$; unpaired Student's t test.

suggesting a link between PARylation and BRCA1 levels. In oxidant-treated *PRDX1* KO cells, persistent SSB-induced hyper-PARylation might promote a reduction of selected DNA-repair proteins, including BCRA1, to guide repair toward PARP1-dependent pathways, such as base-excision repair. Because this repair machinery was overwhelmed in *PRDX1* KO cells, the PARP1-mediated inactivation of HR may have led to accumulation of telomeric fragments. Inhibition of the poly(ADP-ribose)-catabolizing enzyme PARG elevates PARylation and was shown to suppress all known DSB-repair pathways, which include C-NHEJ, Alt-NHEJ, and HR (Chen and Yu, 2019). PARylation is considered to trap repair proteins at the vicinity of damaged sites, blocking the traffic of repair proteins at the site of damage.

The mechanism of PARP-dependent reduction of BRCA1 upon oxidative stress in *PRDX1* KO cells remains unclear. PRDX1 has been reported to shield certain proteins from ROS-induced degradation and inactivation. For example, PRDX1 interacts and stabilizes androgen receptor (AR) during oxidative stress, thereby promoting AR signaling (Feng et al., 2020). PRDX1 also binds to the tumor suppressor PTEN, safeguarding it from oxidative-stress-induced inactivation (Cao et al., 2009). Therefore, it is possible that PRDX1 directly interacts with BRCA1 to shield it from oxidative stress. However, our attempts to detect an interaction between PRDX1 and BRCA1 failed, and we also could not detect PARylated forms of BRCA1 in *PRDX1* KO cells upon oxidative stress (data not shown). Irrespective of the mechanism that regulates BRCA1, PRDX1 seems to protect its levels under oxidative stress, which is crucial for HR-mediated suppression of genome instability.

Cancer cells are more susceptible to ROS than non-cancer cells, providing an opportunity to preferentially target cancer cells by ROS-inducing therapeutics (Sabharwal and Schumacker, 2014). Our observation that oxidant treatment of *PRDX1* KO cells leads to massive telomeric instability, supports the notion that PRDX1 may be used as an anti-cancer target to specifically attack telomeres and potentially enhance the efficacy of ROS-inducing therapeutics and telomerase inhibitors. In such a setting, however, PARP-inhibitors should not be included because they would be predicted to enhance, rather than reduce, the genome stability and viability of cancer cells.

STAR★METHODS

Detailed methods are provided in the online version of this paper and include the following:

- KEY RESOURCES TABLE
- RESOURCE AVAILABILITY
  - Lead contact
  - Materials availability
  - Data and code availability
- EXPERIMENTAL MODEL AND SUBJECT DETAILS
  - Cell lines
- METHOD DETAILS
  - Oxidant treatment and assessment of DNA damage
  - Thymidine block and EdU incorporation assay
  - RAD51 foci detection by immunofluorescence (IF)
  - Chromatin Immunoprecipitation (ChIP)
  - siRNA transfection
  - Immunoblotting
  - Cell cycle analysis
  - RNA isolation and RT–qPCR for quantification of BRCA1 mRNA
- QUANTIFICATION AND STATISTICAL ANALYSIS

SUPPLEMENTAL INFORMATION

Supplemental Information can be found online at https://doi.org/10.1016/j.celrep.2020.108347.

ACKNOWLEDGMENTS

We thank our laboratory members for discussion. Research in the J.L. laboratory was supported by the Swiss National Science Foundation (SNSF grant 310030_184718), the SNSF-funded National Centre of Competence in Research RNA and Disease Network (grant 182880), the Swiss Cancer League (KLS-3824-02-2016), an Innovative Training Network (ITN) (aDDRess) from the European Commission's Seventh Framework Programme (grant 812829) and EPFL.

AUTHOR CONTRIBUTIONS

W.A. and J.L. designed the research, W.A. performed the experiments, and J.L. and W.A. wrote the manuscript.

DECLARATION OF INTERESTS

The authors declare no competing interests.

Received: March 31, 2020
Revised: August 26, 2020
Accepted: October 13, 2020
Published: November 3, 2020

REFERENCES

Aeby, E., Ahmed, W., Redon, S., Simanis, V., and Lingner, J. (2016). Peroxiredoxin 1 protects telomeres from oxidative damage and preserves telomeric DNA for extension by telomerase. Cell Rep. *17*, 3107–3114.

Ahmed, W., and Lingner, J. (2018a). Impact of oxidative stress on telomere biology. Differentiation *99*, 21–27.

Ahmed, W., and Lingner, J. (2018b). PRDX1 and MTH1 cooperate to prevent ROS-mediated inhibition of telomerase. Genes Dev. *32*, 658–669.

Beck, C., Robert, I., Reina-San-Martin, B., Schreiber, V., and Dantzer, F. (2014). Poly(ADP-ribose) polymerases in double-strand break repair: focus on PARP1, PARP2 and PARP3. Exp. Cell Res. *329*, 18–25.

Bjursell, G., and Reichard, P. (1973). Effects of thymidine on deoxyribonucleoside triphosphate pools and deoxyribonucleic acid synthesis in Chinese hamster ovary cells. J. Biol. Chem. *248*, 3904–3909.

Bryant, H.E., Schultz, N., Thomas, H.D., Parker, K.M., Flower, D., Lopez, E., Kyle, S., Meuth, M., Curtin, N.J., and Helleday, T. (2005). Specific killing of BRCA2-deficient tumours with inhibitors of poly(ADP-ribose) polymerase. Nature *434*, 913–917.

Caldecott, K.W. (2008). Single-strand break repair and genetic disease. Nat. Rev. Genet. *9*, 619–631.

Cao, J., Schulte, J., Knight, A., Leslie, N.R., Zagozdzon, A., Bronson, R., Manevich, Y., Beeson, C., and Neumann, C.A. (2009). Prdx1 inhibits tumorigenesis via regulating PTEN/AKT activity. EMBO J. *28*, 1505–1517.

Caron, M.C., Sharma, A.K., O'Sullivan, J., Myler, L.R., Ferreira, M.T., Rodrigue, A., Coulombe, Y., Ethier, C., Gagne, J.P., Langelier, M.F., et al. (2019). Poly(ADP-ribose) polymerase-1 antagonizes DNA resection at double-strand breaks. Nat. Commun. *10*, 2954.

Ceccaldi, R., Rondinelli, B., and D'Andrea, A.D. (2016). Repair pathway choices and consequences at the double-strand break. Trends Cell Biol. *26*, 52–64.

Chen, S.H., and Yu, X. (2019). Targeting dePARylation selectively suppresses DNA repair-defective and PARP inhibitor-resistant malignancies. Sci Adv. *5*, eaav4340.

Chung, Y.M., Yoo, Y.D., Park, J.K., Kim, Y.T., and Kim, H.J. (2001). Increased expression of peroxiredoxin II confers resistance to cisplatin. Anticancer Res. *21*, 1129–1133.

Coluzzi, E., Colamartino, M., Cozzi, R., Leone, S., Meneghini, C., O'Callaghan, N., and Sgura, A. (2014). Oxidative stress induces persistent telomeric DNA damage responsible for nuclear morphology change in mammalian cells. PLoS ONE *9*, e110963.

de Lange, T. (2009). How telomeres solve the end-protection problem. Science *326*, 948–952.

Dekhuijzen, P.N. (2004). Antioxidant properties of N-acetylcysteine: their relevance in relation to chronic obstructive pulmonary disease. Eur. Respir. J. *23*, 629–636.

Diehn, M., Cho, R.W., Lobo, N.A., Kalisky, T., Dorie, M.J., Kulp, A.N., Qian, D., Lam, J.S., Ailles, L.E., Wong, M., et al. (2009). Association of reactive oxygen species levels and radioresistance in cancer stem cells. Nature *458*, 780–783.

Doksani, Y., and de Lange, T. (2016). Telomere-internal double-strand breaks are repaired by homologous recombination and PARP1/Lig3-dependent end-joining. Cell Rep. *17*, 1646–1656.

El-Khamisy, S.F., Masutani, M., Suzuki, H., and Caldecott, K.W. (2003). A requirement for PARP-1 for the assembly or stability of XRCC1 nuclear foci at sites of oxidative DNA damage. Nucleic Acids Res. *31*, 5526–5533.

Eustermann, S., Wu, W.F., Langelier, M.F., Yang, J.C., Easton, L.E., Riccio, A.A., Pascal, J.M., and Neuhaus, D. (2015). Structural basis of detection and signaling of dna single-strand breaks by human PARP-1. Mol. Cell *60*, 742–754.

Farmer, H., McCabe, N., Lord, C.J., Tutt, A.N., Johnson, D.A., Richardson, T.B., Santarosa, M., Dillon, K.J., Hickson, I., Knights, C., et al. (2005). Targeting the DNA repair defect in BRCA mutant cells as a therapeutic strategy. Nature *434*, 917–921.

Feng, T., Zhao, R., Sun, F., Lu, Q., Wang, X., Hu, J., Wang, S., Gao, L., Zhou, Q., Xiong, X., et al. (2020). TXNDC9 regulates oxidative stress-induced androgen receptor signaling to promote prostate cancer progression. Oncogene *39*, 356–367.

Fisher, A.E., Hochegger, H., Takeda, S., and Caldecott, K.W. (2007). Poly(-ADP-ribose) polymerase 1 accelerates single-strand break repair in concert with poly(ADP-ribose) glycohydrolase. Mol. Cell. Biol. *27*, 5597–5605.

Fouquerel, E., Lormand, J., Bose, A., Lee, H.T., Kim, G.S., Li, J., Sobol, R.W., Freudenthal, B.D., Myong, S., and Opresko, P.L. (2016). Oxidative guanine base damage regulates human telomerase activity. Nat. Struct. Mol. Biol. *23*, 1092–1100.

Fouquerel, E., Barnes, R.P., Uttam, S., Watkins, S.C., Bruchez, M.P., and Opresko, P.L. (2019). Targeted and persistent 8-oxoguanine base damage at telomeres promotes telomere loss and crisis. Mol. Cell *75*, 117–130.e116.

Gerasimenko, J.V., Gerasimenko, O.V., Palejwala, A., Tepikin, A.V., Petersen, O.H., and Watson, A.J. (2002). Menadione-induced apoptosis: roles of cytosolic Ca^{2+} elevations and the mitochondrial permeability transition pore. J. Cell Sci. *115*, 485–497.

Grolimund, L., Aeby, E., Hamelin, R., Armand, F., Chiappe, D., Moniatte, M., and Lingner, J. (2013). A quantitative telomeric chromatin isolation protocol identifies different telomeric states. Nat. Commun. *4*, 2848.

Hanzlikova, H., Gittens, W., Krejcikova, K., Zeng, Z., and Caldecott, K.W. (2017). Overlapping roles for PARP1 and PARP2 in the recruitment of endogenous XRCC1 and PNKP into oxidized chromatin. Nucleic Acids Res. *45*, 2546–2557.

Hu, Y., Petit, S.A., Ficarro, S.B., Toomire, K.J., Xie, A., Lim, E., Cao, S.A., Park, E., Eck, M.J., Scully, R., et al. (2014). PARP1-driven poly-ADP-ribosylation regulates BRCA1 function in homologous recombination-mediated DNA repair. Cancer Discov. *4*, 1430–1447.

Kim, S.K., Yang, J.W., Kim, M.R., Roh, S.H., Kim, H.G., Lee, K.Y., Jeong, H.G., and Kang, K.W. (2008). Increased expression of Nrf2/ARE-dependent antioxidant proteins in tamoxifen-resistant breast cancer cells. Free Radic. Biol. Med. *45*, 537–546.

Kuzminov, A. (2001). Single-strand interruptions in replicating chromosomes cause double-strand breaks. Proc. Natl. Acad. Sci. USA *98*, 8241–8246.

Lazzerini-Denchi, E., and Sfeir, A. (2016). Stop pulling my strings—what telomeres taught us about the DNA damage response. Nat. Rev. Mol. Cell Biol. *17*, 364–378.

Loor, G., Kondapalli, J., Schriewer, J.M., Chandel, N.S., Vanden Hoek, T.L., and Schumacker, P.T. (2010). Menadione triggers cell death through ROS-dependent mechanisms involving PARP activation without requiring apoptosis. Free Radic. Biol. Med. *49*, 1925–1936.

Lord, C.J., and Ashworth, A. (2017). PARP inhibitors: synthetic lethality in the clinic. Science *355*, 1152–1158.

Neumann, C.A., Krause, D.S., Carman, C.V., Das, S., Dubey, D.P., Abraham, J.L., Bronson, R.T., Fujiwara, Y., Orkin, S.H., and Van Etten, R.A. (2003). Essential role for the peroxiredoxin Prdx1 in erythrocyte antioxidant defense and tumour suppression. Nature *424*, 561–565.

Neumann, C.A., Cao, J., and Manevich, Y. (2009). Peroxiredoxin 1 and its role in cell signaling. Cell Cycle *8*, 4072–4078.

Noh, D.Y., Ahn, S.J., Lee, R.A., Kim, S.W., Park, I.A., and Chae, H.Z. (2001). Overexpression of peroxiredoxin in human breast cancer. Anticancer Res. *21*, 2085–2090.

Oikawa, S., and Kawanishi, S. (1999). Site-specific DNA damage at GGG sequence by oxidative stress may accelerate telomere shortening. FEBS Lett. *453*, 365–368.

Park, J.H., Kim, Y.S., Lee, H.L., Shim, J.Y., Lee, K.S., Oh, Y.J., Shin, S.S., Choi, Y.H., Park, K.J., Park, R.W., et al. (2006). Expression of peroxiredoxin and thioredoxin in human lung cancer and paired normal lung. Respirology *11*, 269–275.

Perkins, A., Nelson, K.J., Parsonage, D., Poole, L.B., and Karplus, P.A. (2015). Peroxiredoxins: guardians against oxidative stress and modulators of peroxide signaling. Trends Biochem. Sci. *40*, 435–445.

Ray Chaudhuri, A., and Nussenzweig, A. (2017). The multifaceted roles of PARP1 in DNA repair and chromatin remodelling. Nat. Rev. Mol. Cell Biol. *18*, 610–621.

Saada, A., Lambert, S.A.E., and Carr, A.M. (2018). Preserving replication fork integrity and competence via the homologous recombination pathway. DNA Repair (Amst.) *71*, 135–147.

Sabharwal, S.S., and Schumacker, P.T. (2014). Mitochondrial ROS in cancer: initiators, amplifiers or an Achilles' heel? Nat Rev Cancer 14, 709-721. Biol. Med. (Aligarh) *49*, 1925–1936.

Satoh, M.S., and Lindahl, T. (1992). Role of poly(ADP-ribose) formation in DNA repair. Nature *356*, 356–358.

Schultz, N., Lopez, E., Saleh-Gohari, N., and Helleday, T. (2003). Poly(ADP-ribose) polymerase (PARP-1) has a controlling role in homologous recombination. Nucleic Acids Res. *31*, 4959–4964.

Sotgia, F., Martinez-Outschoorn, U.E., and Lisanti, M.P. (2011). Mitochondrial oxidative stress drives tumor progression and metastasis: should we use antioxidants as a key component of cancer treatment and prevention? BMC Med. *9*, 62.

von Zglinicki, T. (2002). Oxidative stress shortens telomeres. Trends Biochem. Sci. *27*, 339–344.

Xie, S., Mortusewicz, O., Ma, H.T., Herr, P., Poon, R.Y., Helleday, T., and Qian, C. (2015). Timeless interacts with PARP-1 to promote homologous recombination repair. Mol. Cell *60*, 163–176.

Yang, H., Villani, R.M., Wang, H., Simpson, M.J., Roberts, M.S., Tang, M., and Liang, X. (2018). The role of cellular reactive oxygen species in cancer chemotherapy. J. Exp. Clin. Cancer Res. *37*, 266.

STAR★METHODS

KEY RESOURCES TABLE

REAGENT or RESOURCE	SOURCE	IDENTIFIER
Antibodies		
Mouse monoclonal anti-BRCA1	Santa Cruz Biotechnology	Cat# sc-6954; RRID: AB_626761
Mouse monoclonal anti-Tubulin	Sigma-Aldrich	Cat#T9026; RRID: AB_477593
Rabbit monoclonal anti-Vinculin	Abcam	Cat# ab129002, RRID:AB_11144129
Rabbit monoclonal anti-OGG1	Abcam	Cat# ab124741, RRID: AB_10973360
Rabbit monoclonal anti-RAD51	Abcam	Cat# ab133534, RRID: AB_2722613
Mouse monoclonal anti-γH2AX	Millipore	Cat# 05-636; cloneJBW301; RRID: AB_309864
Rabbit polyclonal anti-PARP1	Abcam	Cat# ab194586
Mouse monoclonal anti-Poly (ADP-ribose)	Enzo Life Sciences	Cat# ALX-804-220-R100, RRID: AB_2052275
Mouse monoclonal anti-hnRNPA1	Santa Cruz Biotechnology	Cat# sc-32301; clone 4B10; RRID: AB_627729
Anti-Mouse IgG (H+L) HRP conjugated	Promega	Cat# W4021; RRID: AB_430834
Anti-Rabbit IgG (H+L) HRP conjugated	Promega	Cat#W4011; RRID: AB_430833
Anti-Rabbit IgG (H+L) Alexa Flour 488 conjugated	ThermoFischer Scientific	Cat# A-11008, RRID: AB_143165
Chemicals, Peptides and Recombinant Proteins		
Bovine Serum Albumin	Sigma-Aldrich	Cat# A7906
Puromycin	InvivoGen	Cat# ant-pr-1
Lipofectamine 2000 Transfection reagents	ThermoFischer Scientific	Cat# 11668019
Lipofectamine RNAiMAX Transfection reagent	ThermoFischer Scientific	Cat# 13778150
Formaldehyde	ThermoFischer Scientific	Cat# 28908
Protein G Sepharose	GE Healthcare	Cat# 17061805
EdU (5-ethynyl-2′-deoxyuridine)	ThermoFischer Scientific	Cat# E10187
Alexa Flour™ 647 Azide, triethylammonium Salt	ThermoFischer Scientific	Cat# A10277
DAPI	Sigma-Aldrich	Cat# D9542
RAD51 Inhibitor (B02)	Sigma-Aldrich	Cat# SML0364
PARG inhibitor: Adenosine 5′-diphosphate (hydroxymethyl) pyrrolidinediol.NH4.2H_2O (ADP-HPD ammonium salt.dihydrate)	Sigma-Aldrich	Cat# 118415
Talazoparib (BMN 673)	Selleckchem	Cat# S7048
Olaparib (AZD2281)	Selleckchem	Cat# S1060
Veliparib (ABT-888)	Selleckchem	Cat# S1004
N-acetyl-L-cysteine	Sigma-Aldrich	Cat# A7250
Hydrogen peroxide Solution	Sigma-Aldrich	Cat#H1009
Menadione sodium bisulfite	Sigma-Aldrich	Cat# M5750
Thymidine	Sigma-Aldrich	Cat# T1895
Propidium Iodide	Sigma-Aldrich	Cat# 4170
HphI	New England Biolabs	Cat# R0158S
HinfI	New England Biolabs	Cat# R0155S
MnlI	New England Biolabs	Cat# R0163S
RsaI	New England Biolabs	Cat# R0167S
AluI	New England Biolabs	Cat# R0137S

(*Continued on next page*)

Continued

REAGENT or RESOURCE	SOURCE	IDENTIFIER
CutSmart Buffer	New England Biolabs	Cat# B7204S
Experimental Models: Cell Lines		
HCT116 Population	ATCC	Cat#CCL-247; RRID: CVCL_0291
HCT116 PRDX1 KO	Aeby et al., 2016	PMID: 28009281
HCT116 WT	This Paper	N/A
HeLa	Lingner Lab	N/A
Oligonucleotides		
siGFP targeting sequence: GCAGCACGACUUCUUCAAGUU	This paper	N/A
siOGG1 targeting sequence #1: GUAUGGACACUGACUCAGACU	This paper	N/A
siOGG1 targeting sequence #2: GAUCAAGUAUGGACACUGA	Ambion	Cat# 4390824; ID:s9836
siPARP1 targeting sequence: CCGAGAAATCTCTTACCTCAA	Xie et al., 2015	PMID: 26344098
ON-Target plus human RAD51 siRNA	Dharmacon	N/A
qRT-PCR forward primer for BRCA1: GCCACACGATTTGACGGAAAC	This paper	N/A
qRT-PCR reverse primer for BRCA1: GGTCATCAGAGAAGAGGCTGATTC	This paper	N/A
Alu probe sequence GTGATCCGCCCGCCTCGGCCTCCCA AAGTG	This Paper	N/A
Software and Algorithms		
AIDA image analyzer	Elysia Raytest	http://www.elysia-raytest.com/de/
GraphPad Prism 7	Graph Pad	https://www.graphpad.com
Fiji-ImageJ	NIH	https://fiji.sc
Accuri C6 sample analyzer	BD Biosciences	https://www.bdbiosciences.com/en-us/instruments/research-instruments/research-cell-analyzers/accuri-c6-plus
Axiovision 4.2	Carl Zeiss	http://www.zeiss.com/microscopy/int/downloads.html?vaURL=www.zeiss.com/microscopy/int/downloads/axiovision-downloads.html

RESOURCE AVAILABILITY

Lead contact

Further information and requests for reagents may be directed to lead author Joachim Lingner (joachim.lingner@epfl.ch).

Materials availability

All the cell lines generated and used in this study are available on request from the lead contact, Joachim Lingner (joachim.lingner@epfl.ch).

Data and code availability

All the raw data associated with this study are available on request from the lead contact, Joachim Lingner (joachim.lingner@epfl.ch).

EXPERIMENTAL MODEL AND SUBJECT DETAILS

Cell lines

Human HCT116 and HeLa cell lines were used for all experiments and genetic manipulations. All cells were cultured in DMEM supplemented with 10% FBS and maintained in an incubator at 37°C in presence of 5% CO_2. Generation of HCT116 *PRDX1* KO cell lines

is described in Aeby et al., 2016. A HCT116 WT clone with comparable telomere length as the *PRDX1 KO* clone was isolated by single cell dilution in a 96-well plate in this study.

METHOD DETAILS

Oxidant treatment and assessment of DNA damage

Cells were treated with 1 mM menadione or H_2O_2 for 30 min to induce DNA damage. Following oxidant treatment, cells were washed with pre-warmed PBS and incubated in fresh complete DMEM supplemented with or without 5 mM NAC for indicated time intervals.

For in-gel analysis of telomeric DNA, genomic DNA was purified from cells using the Wizard genomic DNA purification kit (Promega). 6 μg of genomic DNA was subjected to restriction digestion with HinfI and RsaI (10 U of each) in a 50 μL reaction volume containing 1 × CutSmart buffer (New England Biolabs). For Single Strand Break (SSB) analysis, 2 μg of digested DNA was fractionated on 0.8% agarose gels containing 50 mM NaOH and 1 mM EDTA by gel electrophoresis at 2 V/cm for 16 h. Subsequently, the gels were treated with neutralization buffer (0.5 M Tris-HCl at pH 7.5, 1.5 M NaCl) for 45 min and dried on a gel dryer for 2 h. For native TRF gel analysis, 2 μg of digested DNA per lane was resolved on 0.8% agarose gels in 1 × TBE and dried as described above. Dried gels were treated for 30 min first with denaturation buffer (0.5 M NaOH, 1.5 M NaCl) and then with neutralization buffer (0.5 M Tris-HCl at pH 7.5, 1.5 M NaCl) before prehybridization with Church mix for 2 h and overnight incubation at 50°C with randomly labeled TeloC probe (Grolimund et al., 2013). After hybridization, the gels were washed at 50°C (once with 4 × SSC, once with 4 × SSC + 0.1% SDS, and twice with 2 × SSC + 0.1% SDS) and exposed to a phosphorimager screen overnight. After exposure, screens were scanned on a Typhoon phosphorimager (GE). Telomere length was quantified based on densitometry using AIDA software. The intensity/abundance of telomere fragments was measured within the lane by drawing a densitometry calculation box using AIDA software, which encompasses all telomere fragments distributed over the lane. The size of telomere fragments at corresponding positions of the lane were deduced by comparing and extrapolating the data from the defined molecular markers loaded in other lanes of the same gel. The average telomere length was obtained as $\Sigma(\text{Inti})/\Sigma(\text{Inti/MWi})$. Inti = intensity of telomere fragments, MW = deduced molecular weight of telomere fragments. The calculation of DNA damage (both SSBs and DSBs) was performed by measuring the percentage decrease in telomere length of treated samples compared to untreated samples. DNA damage is represented as damage/kb which was obtained by dividing the percentage decrease in telomere length by the average telomere length (kb) of the untreated sample. The data were analyzed and plotted by GraphPad Prism 7.

Thymidine block and EdU incorporation assay

WT and *PRDX1* KO cell lines grown on coverslips were treated with 2 mM thymidine for 24 h. After 24 h of persistent thymidine treatment, cells were incubated with EdU (10 μM) for 2 h followed by fixation in 4% formaldehyde. Fixed cells were washed, permeabilized with 0.1% Triton X-100 and incubated with staining solution (4 mM $CuSO_4$, 10 μM Alexa Flour™ 647 Azide and 100 mM sodium ascorbate) for 30 min to trigger Click-IT reaction mediated labeling of EdU with AlexaFlour-647. The EdU labeled cells were counterstained with DAPI and imaged with a Zeiss Axio plan 2 fluorescence microscope.

RAD51 foci detection by immunofluorescence (IF)

For RAD51 foci detection, HCT116 cells were grown on coverslips for 24 h followed by exposing them to 3 Gy of gamma rays (IR). Irradiated cells were recovered in fresh DMEM medium for 4 h in the presence or absence of 100 μM RAD51 inhibitor (B02) followed by fixation in 4% formaldehyde and permeabilization with 0.1% Triton X-100. The permeabilized cells were blocked and subsequently incubated with anti-RAD51 antibody (1:000 dilution) for 2 h at room temperature and then 1 h with anti-Rabbit Alexa 488 conjugated secondary antibody. Cells were counterstained with DAPI and RAD51 foci were visualized with a Zeiss Axio plan 2 microscope system at 60X magnification. Images were analyzed using Fiji-ImageJ.

Chromatin Immunoprecipitation (ChIP)

For ChIP experiments, cells were treated with 1 mM H_2O_2 for 30 min and harvested after 6 h of recovery in anti-oxidant containing medium. ChIP protocol for γH2AX and RAD51 was performed as described earlier (Aeby et al., 2016). Briefly, 16 million cells per condition were harvested and crosslinked with 1% formaldehyde for 15 min followed by quenching the crosslinking reaction with 125 mM Glycine. The crosslinked cells were lysed in lysis buffer (1% SDS, 10 mM EDTA pH 8.0, 50 mM Tris–Cl pH 8.0, EDTA-free protease inhibitor complex (Roche), centrifuged and subsequently the chromatin fraction was resuspended in LB3 buffer (0.1% Na-deoxycholate, 0.25% sodium lauroyl sarcosinate, 1 mM EDTA pH 8.0, 0.5 mM EGTA pH 8.0, 10 mM Tris-HCl pH 8.0, 200 mM NaCl, cOmplete, EDTA-free (Roche) for sonication in Covaris to fragment the DNA. The lysates were precleared by incubating with Protein-G Sepharose beads and 4 million cell equivalents pre-cleared chromatin fraction was incubated with anti- γH2AX or anti-RAD51 antibody (4 μg) and 40 μL protein-G Sepharose beads overnight. The immunoprecipitated chromatin fractions were extensively washed and subjected to reverse crosslinking by incubating in reverse crosslinking buffer (1% SDS, 0.1 M $NaHCO_3$, 0.5 mM EDTA pH 8.0, 20 mM Tris-HCl pH 8.0, 10 μg DNase-free RNase (Roche) at 65°C overnight. The eluted DNA was purified with the QIAGEN PCR clean up kit and subsequently blotted on Hybond N+ (Amersham) nylon membrane and probed with a radiolabeled telomeric DNA specific probe (TeloC). The telomeric DNA signals were visualized with a phosphorimager, quantified by AIDA software and analyzed by GraphPad prism 7.0.

siRNA transfection

0.6 million HCT116 cells were seeded into 6-well plate 16 h prior to transfection. 20 nM targeting siRNA or control siGFP was transfected using Lipofectamine RNAiMAX Reagent (ThermoFischer Scientific). After 48 h, cells were expanded in 10 cm dishes and 24 h later processed for downstream analyses.

Immunoblotting

Cell pellets were resuspended in RIPA lysis buffer and sonicated, and protein amounts were quantified using the BCA assay kit (Pierce). 40 μg of cell lysates were boiled for 5 min in 1X Laemmli buffer and resolved on 4%–20% Mini Protean TGX (Bio-Rad). Proteins were transferred to nitrocellulose blotting membranes (Amersham), blocked with blocking solution (5% non-fat dry milk in PBS/0.1% Tween 20) for 30 min, and incubated with the appropriate primary antibody in blocking solution overnight at 4°C. The membranes were washed three times for 5 min with PBS/0.1% Tween-20 followed by incubation with HRP conjugated secondary antibody (Promega) and chemiluminescence detection using a western blotting detection kit (Western bright ECL, Advansta).

Cell cycle analysis

For cell cycle distribution analysis cells were stained with propidium iodide (PI) and analyzed by flow cytometry. For each sample, $2x10^6$ cells were pelleted, washed in 1xPBS and fixed by dropwise addition of 1 mL of ice-cold 70% ethanol and incubated overnight. Following the fixation, cells were resuspended in 250 μL 1xPBS containing 0.2 μg/mL of RNase A and incubated for 15 min at 37°C. Cells were then stained by addition of 250 μL of 1xPBS containing 80 μg/mL PI and incubated at 4°C for 10 min. Subsequently, cells were passed through a strainer and analyzed on Accuri C6 (BD Biosciences). The percentage of cells in each phase of the cell cycle was determined using the Accuri C6 sample analysis program.

RNA isolation and RT–qPCR for quantification of BRCA1 mRNA

Total RNA was isolated form 3×10^6 cells following the manufacturer's recommendations (Macherey-Nagel). The residual DNA was removed with 3 DNase treatment steps and cDNA from three independent biological replicates was synthesized using Luna® Universal One-Step RT-qPCR Kit (New England Biolabs) from 2 μg of total RNA in a 20 μl final reaction volume. The cDNA was diluted to 50 μl and subsequently used for setting up quantitative PCR (qPCR) on an Applied Biosystems 7900HT Fast Real-Time System exploiting Power SYBR

Green PCR Master Mix (Applied Biosystems) in a 384-well reaction plate. Each sample was prepared in three biological and two technical replicates. The master mix for each reaction was prepared as follows: 2 μl diluted cDNA, 5 pmol of forward primer, 5 pmol reverse primer, 1 × Power SYBR Green PCR Master Mix, and H_2O to a total volume of 10 μl. qPCR data were analyzed using the relative $2^{-\Delta\Delta Ct}$ quantification method, and GAPDH was used for the normalization.

QUANTIFICATION AND STATISTICAL ANALYSIS

Statistical parameters, statistical tests used, standard deviation, and statistical significance are included in each figure's legend. Statistical analysis was carried out using Graphpad Prism 7 software, and differences were considered statistically significant when $p < 0.05$ by two tailed Student's t test.